This article has been accepted for publication in a future proceedings of this conference, but has not been fully edited. Content may change prior to final publication.
Citation information: DOI: 10.1109/CPERE65146.2025.11240016, 2025 IEEE Conference on Power Electronics and Renewable Energy (CPERE)

Inverter-Side Current Feedback Active Damping Based on Phase-Lead Compensation for Grid-Connected Inverter

Li Zhang
School of Electrical and Power Engineering
Hohai University
Nanjing, China
zhanglinuaa@hhu.edu.cn

Aijun Qin
School of Electrical and Power Engineering
Hohai University
Nanjing, China
qinaijun@hhu.edu.cn

Qiang Qian
School of Electrical and Power Engineering
Hohai University
Nanjing, China
qianqiang@hhu.edu.cn

Ahmed F. Zobaa
College of Engineering, Design and Physical Sciences
Brunel University of London
Uxbridge, U.K.
azobaa@ieee.org

Sobhy Mohamed Abdelkader
Department of Electrical Power Engineering
Egypt-Japan University of Science and Technology
New Borg El-Arab, Egypt
sobhy.abdelkader@ejust.edu.eg

Diaa-Eldin A. Mansour
Department of Electrical Power Engineering
Egypt-Japan University of Science and Technology
New Borg El-Arab, Egypt
diaa.mansour@ejust.edu.eg

***Abstract*—To suppress the resonance in LCL-type grid-connected inverter (GCI), various active damping (AD) methods have been developed. In this article, an inverter-side current feedback active damping (ICFB-AD) strategy with phase-lead compensation is proposed, which achieves both resonance attenuation and accurate current control. A second-order unstable phase-lead filter is introduced in series with the ICFB loop to enhance the stability and robustness of the GCI. Design guidelines for the second-order unstable PLF are also presented. The proposed system ensures stability across a wide range of LCL resonance frequencies and exhibits strong robustness against variations in the filter inductance and grid impedance. Finally, the effectiveness of the proposed ICFB-AD strategy, along with its *z*-domain design methodology, is validated by experimental results.**

Keywords—active damping, digital control delay, phase compensation, grid-connected inverter, LCL filter

I. INTRODUCTION

The LCL filter is widely adopted in grid-connected inverters (GCI) due to its advantages such as compact size, low cost, and strong attenuation of switching harmonics generated by power semiconductor devices. However, the high gain and -180° phase shift at the resonant frequency of the LCL filter may lead to instability in the GCI system. Therefore, active damping (AD) methods are required to suppress resonance[1]. Nevertheless, digital control delay (DCD) significantly weakens the performance of AD [2]. A practical way to mitigate the adverse effects of DCD is through phase compensation. Delay compensation methods can be mainly categorized into two approaches: one is the sampling modification method, which reduces delay by adjusting the sampling or loading instants; the other is phase-lead compensation through dedicated digital filters.

Sampling modification is the most straightforward way to reduce DCD, commonly implemented through multi-sampling or real-time sampling [3]. Multi-sampling reduces the computational delay by increasing the sampling frequency. In [4], an eight-times-per-switching-cycle sampling method reduces the control delay from $1.5T_{sw}$ to $3T_{sw}/16$. However, this method inevitably introduces switching noise and suffers from aliasing effects [5]. To suppress these effects, repetitive control filters can be used to filter out switching harmonics [6][7]. Nevertheless, such filters also introduce phase lag, which weakens the damping of high-frequency resonant peaks.

Real-time sampling reduces delay by aligning the sampling instant with the carrier loading time [8]. In [9], a generalized real-time computing method under a dual-sampling model is proposed, which eliminates the computational delay. Sampling at the waveform peaks and troughs avoids switching noise interference but requires high computational performance of the digital controller. In contrast, modulation strategies with half-sample delay configurations offer a balance between delay reduction and practical feasibility [10][11].

Phase-lead compensation, on the other hand, mitigates DCD by introducing a phase-lead filter into the control loop. In [12] and[13], the application of second-order generalized integrators (SOGI) and non-ideal SOGI in state-variable-feedback AD is investigated. A digital differentiator based on a generalized integrator is proposed to extend the positive damping frequency range up to $f_s/4$. However, a trade-off must be made between high-frequency gain and phase lead angle during parameter design. First-order phase lead filter [14] or second-order phase lead filter [15] can also be used to compensate for digital control delays. To further enhance GCI robustness, [16] proposes phase compensation for AD using a second-order unstable phase-lead filter, which extends the positive damping frequency range to $(0, f_s/2)$. It is worth noting that the filter is unstable, and the damping loop behaves as a non-minimum phase system. Its applicability to other state-feedback-based AD methods is constrained by stability criteria. AD control strategy based on inverter-side current dual-loop feedback achieves both current control and resonance suppression[17], [18], [19], but the frequency range

This work was supported in part by the National Natural Science Foundation of China under Grant 52322705, in part by the Natural Science Foundation of Jiangsu Province under Grant BK20230037, and in part by the special fund of Jiangsu Province for the Transformation of Scientific and Technological Achievements under Grant BA2023108.

This article has been accepted for publication in a future proceedings of this conference, but has not been fully edited. Content may change prior to final publication.
Citation information: DOI: 10.1109/CPERE65146.2025.11240016, 2025 IEEE Conference on Power Electronics and Renewable Energy (CPERE)

that provides positive damping remains limited under the influence of DCD.

Since the inverter-side current is already measured for overcurrent protection, ICFB-AD becomes a cost-effective and practical approach for engineering applications [20][21]. In this paper, a coordinated design combining sampling modification and phase compensation is proposed, resulting in an ICFB-AD strategy based on phase-lead compensation. This method significantly improves the stability and robustness of the GCI. Finally, the correctness of the theoretical analysis is verified by experimental results.

II. Impacts of Digital Control Delay on the AD of LCL-Type GCI

A. System description

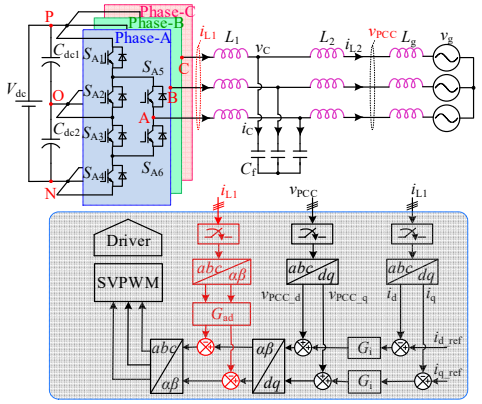

Fig. 1 Block diagram of the ICFB-AD control system

Fig. 1 shows the block diagram of the ICFB-AD control system. The LCL filter consists of the inverter-side inductor L_1, the AC filter capacitor C_f, and the grid-side inductor L_2. The grid is modeled as an ideal voltage source v_g in series with the grid impedance Z_g, which includes transmission line impedance and transformer leakage inductance. The resistive component of Z_g provides inherent damping. To consider the worst-case scenario, Z_g is assumed to be purely inductive, i.e., $Z_g = L_g$, and the total grid-side inductance is defined as $L_T = L_2 + L_g$. The GCI output power is controlled through the inverter-side current i_{L1}, which is transformed into the dq frame and compared with the reference values i_{d_ref} and i_{q_ref}. The resulting errors are fed into the current controller G_i. The point of common coupling (PCC) voltage v_{PCC}, after being transformed into the dq frame, is added to the output of the current controller to reduce inrush current during inverter startup. The PLF is inserted in the inverter-side current feedback path to damp the resonance peak of the LCL filter.

B. Equivalent Virtual Impedance Model

According to Fig. 1, the control block diagram of the ICFB-AD is illustrated in Fig. 2(a), where $v_{inv}(s)$ is the inverter output voltage, $i_{L1\_ref}(s)$ is the current reference, and $G_{ad}(s)$ denotes the phase-leading filter PLF. In the AD inner loop, the inverter-side current i_{L1} is processed by $G_{ad}(s)$ to damp the resonance peak of the LCL filter. In the outer loop, i_{L1} is also used to control the inverter output power. Therefore, the system forms a dual-loop control structure based on the inverter-side current.

The transfer function from the v_{inv} to the inverter-side current i_{L1} can be expressed as:

$$G_{iL1}(s) = \frac{i_{L1}(s)}{v_{inv}(s)} = \frac{1 + L_T C_f s^2}{L_1 L_T C_f s\left(s^2 + \omega_r^2\right)} \tag{1}$$

where, ω_r represents the resonance angular frequency of the LCL filter, which is given by:

$$\omega_r = 2\pi f_r = \sqrt{\frac{L_1 + L_T}{L_1 L_T C_f}} \tag{2}$$

$G_d(s)$ represents the digital control delay. The PWM modulation delay is approximately half of the sampling period T_s, and the time difference between the sampling moment and the loading moment is the computational delay (λT_s). $G_d(s)$ can be expressed as:

$$G_d(s) = e^{-(0.5+\lambda)sT_s} \tag{3}$$

From Fig. 2(b), the ICFB-AD can be equivalently represented as a series impedance Z_{eq} on the filter inductance L_1. The equivalent virtual impedance is expressed as:

$$\begin{aligned} Z_{eq}(s) &= G_d(s) G_{ad}(s) \\ &= e^{-(0.5+\lambda)sT_s} G_{ad}(s) \end{aligned} \tag{4}$$

Substitute $s=j\omega$ into equation (4):

$$\begin{aligned} Z_{eq}(\omega) &= \left\{ \begin{matrix} \cos\left[(0.5+\lambda)\omega T_s\right] \\ -j\sin\left[(0.5+\lambda)\omega T_s\right] \end{matrix} \right\} G_{ad}(\omega) \\ &\triangleq R_{eq}(\omega) + jX_{eq}(\omega) \end{aligned} \tag{5}$$

where,

$$\begin{aligned} R_{eq}(\omega) &= G_{ad}(\omega)\cos\left[(0.5+\lambda)\omega T_s\right] \\ X_{eq}(\omega) &= -G_{ad}(\omega)\sin\left[(0.5+\lambda)\omega T_s\right] \end{aligned} \tag{6}$$

From (5), it can be seen that the equivalent resistance R_{eq} and equivalent reactance X_{eq} are the real and imaginary parts of the equivalent impedance Z_{eq}, respectively. The equivalent resistance R_{eq} helps to damp the LCL resonance. As shown in (6), the larger the value of R_{eq}, the stronger the damping effect. However, the configuration of the computational delay λ will alter the frequency range of the positive damping for R_{eq}, while the equivalent reactance X_{eq} will shift the actual resonance frequency.

C. The Principle of Phase Compensation

In practical applications of grid-connected inverters, typical PWM strategies with one-sample or half-sample computational delay configurations are commonly adopted to avoid sampling aliasing and to ensure compatibility between execution time and controller computational capacity.

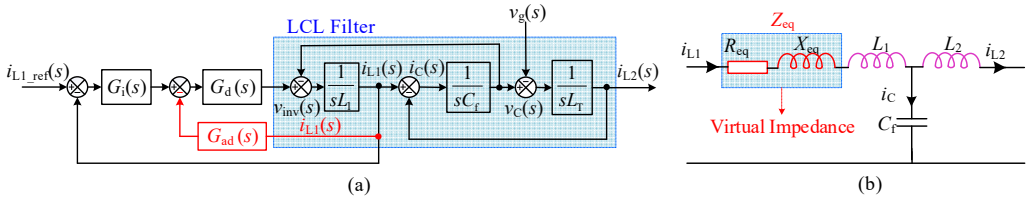

Fig. 2 Equivalent virtual impedance of ICFB-AD. (a) Control block diagram of ICFB-AD. (b) Equivalent virtual impedance

This article has been accepted for publication in a future proceedings of this conference, but has not been fully edited. Content may change prior to final publication.
Citation information: DOI: 10.1109/CPERE65146.2025.11240016, 2025 IEEE Conference on Power Electronics and Renewable Energy (CPERE)

According to (5), by first setting $G_d(s)$ as a proportional link. Fig. 3 shows the complex-plane plots of the equivalent impedance $Z_{eq}(\omega)$ with one-sample and half-sample delay configurations.

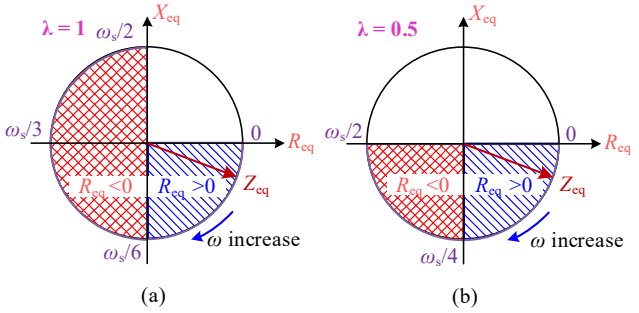

Fig. 3 Complex plane diagram of the equivalent impedance Z_{eq}. (a) $\lambda = 1$. (b) $\lambda = 0.5$.

As shown in Fig. 3(a), when $\lambda = 1$, the positive resistance frequency range of the equivalent resistance R_{eq} is $(0, f_s/6)$. Due to the phase lag introduced by digital control delay, $R_{eq} < 0$ in the frequency range $(f_s/6, f_s/2)$. According to (6), the damping provided in this range becomes negative, which introduces unstable open-loop poles into the dual-loop control system, effectively making it a non-minimum phase system. To ensure that R_{eq} remains positive within $(0, f_s/2)$, phase compensation must be applied over this range, with a 180° phase lead specifically required at $f_s/2$.

As shown in Fig. 3(b), due to the reduction of the computational delay to $\lambda = 0.5$, the positive resistance frequency range of the equivalent resistance R_{eq} is extended to $(0, f_s/4)$, while the negative-resistance region lies within $(f_s/4, f_s/2)$. According to the compensation principle, phase compensation should be performed within the frequency range $(0, f_s/2)$, and a phase lead of only 90° is required at $f_s/2$, so as to further expand the positive-resistance region of R_{eq} up to $f_s/2$.

D. Phase-Leading Filter

To extend the positive damping frequency range of ICFB-AD, a phase lead filter is used for compensation design. According to the phase compensation principle, a second-order unstable phase lead filter $G_{2\_PLF}(s)$ is selected and placed in series with the inverter-side current negative feedback loop. The expression is:

$$G_{2\_PLF}(s) = H_{ad}\frac{s^2 + 2\zeta_\alpha\omega_\alpha s + \omega_\alpha^2}{s^2 - 2\zeta_\beta\omega_\beta s + \omega_\beta^2}, (\omega_\alpha < \omega_\beta) \quad (7)$$

From (7), it can be seen that when $\omega_\alpha < \omega_\beta$, $G_{2\_PLF}(s)$ behaves as a high-pass filter. The numerator of $G_{2\_PLF}(s)$ is a typical second-order system, where ζ_α is the damping ratio, and ω_α is the undamped oscillation frequency. The denominator represents a negative damping second-order system. To ensure that the system has moderate damping and good dynamics, ζ_α and ω_α should be greater than or equal to 0.707.

The phase compensation angle of $G_{2\_PLF}(s)$ can be expressed as:

$$\begin{aligned}\angle G_{2\_PLF}(\omega) &= \arctan\frac{2\zeta_\alpha\omega_\alpha\omega}{\omega_\alpha^2 - \omega^2} + \arctan\frac{2\zeta_\beta\omega_\beta\omega}{\omega_\beta^2 - \omega^2} \\ &= \angle G_{P1}(\omega) + \angle G_{P2}(\omega)\end{aligned} \quad (8)$$

From (8), it can be seen that when $\omega = \omega_\alpha$, $\angle G_{P1}(\omega) = 90°$; when $\omega = \omega_\beta$, $\angle G_{P2}(\omega) = 90°$; and when ω tends to infinity, $G_{2\_PLF}(s)$ provides a maximum phase of 360°. $G_{2\_PLF}(s)$ exhibits a large phase lead, which better satisfies the phase compensation design.

If $\omega_\alpha = \omega_s/4$ and $\omega_\beta = \omega_s/2$ are selected, the phase of the compensated equivalent impedance $Z_{eq}(\omega)$ remains within the range of (−90°, 90°), and it provides better damping performance when the phase of $Z_{eq}(\omega)$ is close to 0°. Therefore, $\omega_\alpha = \omega_s/4$ and $\omega_\beta = \omega_s/2$ are chosen.

It is important to note that $G_{2\_PLF}(s)$ is a second-order unstable element, containing poles in the right half-plane. The phase-lead filter is implemented in the digital controller, so it needs to be discretized. The backward difference discretization method can map the unstable poles in the s-domain to the unit circle in the z-domain. Therefore, $G_{2\_PLF}(s)$ can be designed as a filter in the z-domain, either stable or unstable. When using an unstable filter in series with the damping inner loop feedback path, the damping inner loop behaves as a non-minimum phase system, making its stability design more complex. Therefore, the discretization criteria for the phase-lead filter based on the AD inner loop stability constraints will be explored in the next section.

III. Discrete Domain Modeling and Damping Inner Loop Magnitude-Phase Characteristics Analysis

A. Discrete-Domain Model

According to Fig. 2(a), Fig. 4 illustrates the discrete-domain control block diagram of the ICFB-AD control system, where $z^{-\lambda}$ represents the computational delay of λT_s, and $G_{ad}(z)$ is the discrete form of the phase-leading filter, namely the phase-leading digital filter.

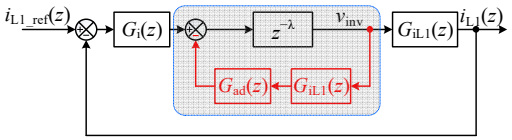

Fig. 4 Discrete-domain control block diagram of the ICFB-AD

Since the conventional Z-transform cannot be directly applied to transfer functions with non-integer sampling delays, an improved Z-transform method is employed to discretize the transfer function [22]. The fractional-order transfer function $G_{iL1}(z)$ from $v_{inv}(z)$ to the inverter-side current $i_{L1}(z)$ is expressed as:

$$G_{iL1}(z) = \frac{z-1}{zL_1L_TC_f}\left\{\begin{array}{l}\dfrac{(1-\lambda)T_sz + \lambda T_s}{\omega_r^2(z-1)^2} + \dfrac{L_TC_f\omega_r^2 - 1}{\omega_r^3} \\ \dfrac{z\sin[(1-\lambda)\omega_rT_s] + \sin(\lambda\omega_rT_s)}{z^2 - 2z\cos(\omega_rT_s) + 1}\end{array}\right\} \quad (10)$$

The open-loop transfer function of the ICFB-AD inner loop is expressed as $T_{AD\_open}(z) = G_{ad}(z)G_{iL1}(z)$, and the closed-

$$T_{AD\_close}(z) = \frac{zL_1(L_1+L_T)\omega_r\cdot(z-1)[z^2 - 2z\cos(\omega_rT_s) + 1]}{zL_1(L_1+L_T)\omega_r\cdot(z-1)[z^2 - 2z\cos(\omega_rT_s) + 1] + \left\{\begin{array}{l}G_{ad}(z)L_1[(1-\lambda)T_sz + \lambda T_s]\cdot[z^2 - 2z\cos(\omega_rT_s) + 1] \\ + L_T[z\sin(\omega_rT_s - \lambda\omega_rT_s) + \sin(\lambda\omega_rT_s)](z-1)^2\end{array}\right\}} \quad (9)$$

This article has been accepted for publication in a future proceedings of this conference, but has not been fully edited. Content may change prior to final publication.
Citation information: DOI: 10.1109/CPERE65146.2025.11240016, 2025 IEEE Conference on Power Electronics and Renewable Energy (CPERE)

loop transfer function of the AD inner loop is given by equation (10).

The open-loop transfer function of the dual-loop control system is expressed as $T_{plant}(z) = G_i(z)T_{AD\_close}(z)G_{iL1}(z)$. From equations (9) and (10), it can be observed that, under any computation delay configuration, the zeros of $T_{AD\_close}(z)$ and the poles of $G_{iL1}(z)$ cancel each other out, and the current regulator $G_i(z)$ does not contain any unstable poles. The outer loop poles of the dual -loop control system are determined by the inner loop $T_{AD\_close}(z)$. Therefore, if the inner loop is designed to be stable, the outer loop does not contain any unstable poles and behaves as a minimum phase system. Hence, the stability of the active damping inner loop is a necessary condition to better meet the stability design of the dual-loop control system.

B. *Magnitude trap in the Damping Inner Loop under Specific Computation Delay*

To analyze the impact of different computation delays on the magnitude and phase characteristics of the damping inner loop, $G_{ad}(z)$ is first set as a proportional element [$G_{ad}(z) = H_{ad}$]. Fig. 5 shows the open-loop bode plot of the ICFB-AD inner loop under different computation delays ($\lambda = 1$ and $\lambda = 0.5$).

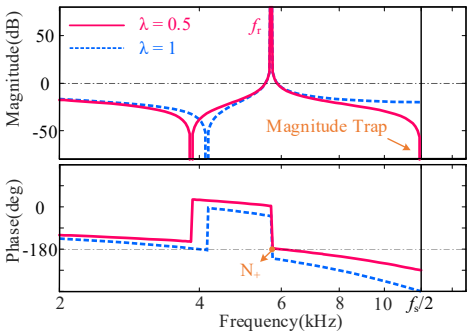

Fig. 5 Open-loop bode diagram of the ICFB-AD inner loop.

From Fig. 5, it can be observed that when $\lambda = 1$, the phase-frequency curve crosses the −180° line at the Nyquist frequency f_N ($f_N = f_s/2$), and the magnitude-frequency curve exhibits a gain of approximately −20dB at f_N. In contrast, when $\lambda = 0.5$, the magnitude-frequency curve exhibits a gain trap at f_N, with the gain being almost infinitely small.

To explain this phenomenon, by substituting $\lambda = 0.5$ into (10), the open-loop transfer function of the damping inner-loop under λ=0.5 is obtained:

$$T_{AD\_open\_\lambda\_0.5} = \frac{G_{ad}(z)(z+1)}{zL_1(L_1+L_2)\omega_r} \cdot \frac{\left\{\begin{array}{c}0.5L_1\omega_r T_s[z^2-2z\cos(\omega_r T_s)+1] \\ +L_2\sin(0.5\omega_r T_s)(z-1)^2\end{array}\right\}}{(z-1)[z^2-2z\cos(\omega_r T_s)+1]} \quad (11)$$

It can be seen that when $\lambda = 0.5$, a factor of $(z+1)$ can be extracted from (11). Substituting $z=e^{j\omega T_s}$ into $(z+1)$, it follows that when $\omega=0.5\omega_s$, $e^{j0.5\omega_s T_s}+1=0$. Therefore, the magnitude gain of the damping inner-loop approaches zero at f_N.

Generally, digital filters exhibit a high-frequency gain issue after discretization, meaning that the magnitude gain of $G_{ad}(z)$ tends to be elevated near f_N. The magnitude trap suppresses the high-frequency gain of $G_{ad}(z)$, preventing the magnitude from remaining above 0 dB when the phase-frequency curve of the damping inner loop crosses −180° at high frequencies. Since configuring $\lambda = 0.5$ can both reduce the computational delay and attenuate the high-frequency gain of $G_{ad}(z)$, this paper adopts $\lambda = 0.5$.

To analyze the design criteria of the digital filter under the effect of the magnitude trap. Fig. 6 presents the open-loop bode plot of the ICFB-AD inner loop after compensation by $G_{2\_PLF}(z)$.

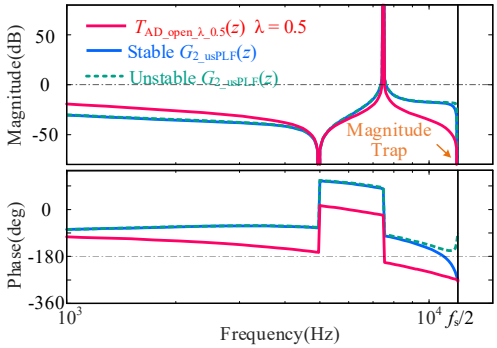

Fig. 6 Open-loop bode diagram of the ICFB-AD inner loop after compensation by $G_{2\_PLF}(z)$.

By applying backward Euler discretization, $G_{2\_PLF}(z)$ can be designed as either stable or unstable. From Fig. 6, when the stable $G_{2\_PLF}(z)$ is cascaded in the inverter-side current feedback path, the damping inner loop forms a minimum-phase system. After phase correction, the phase-frequency curve of the damping loop crosses the −180° line while the magnitude remains below 0 dB, indicating that the inner loop is stable.

In contrast, if $G_{2\_PLF}(z)$ is designed as unstable, the damping inner loop becomes a non-minimum phase system. To ensure inner-loop stability in this case, the phase-frequency curve must cross the −180° phase line multiple times. However, due to the larger high-frequency phase lead provided by the unstable $G_{2\_PLF}(z)$, the phase-frequency curve fails to cross the −180° line, making it impossible to stabilize the damping inner loop.

In conclusion, for ICFB-AD system with $\lambda = 0.5$, a stable digital filter must be used for phase compensation design.

IV. Design of Phase-Lead Compensation Scheme

A. *Design guideline of $G_{2\_PLF}(z)$ parameters*

After applying backward Euler discretization to $G_{2\_PLF}(s)$, the $G_{2\_PLF}(z)$ can be expressed as:

$$G_{2\_PLF}(z) = H_{ad}\frac{A_2z^2+A_1z+A_0}{B_2z^2+B_1z+B_0} \quad (12)$$

where, $A_2 = (T_s\omega_\alpha)^2+2\zeta_\alpha T_s\omega_\alpha+1$, $A_1 = -(2\zeta_\alpha T_s\omega_\alpha+2)$, $A_0 = 1$, $B_2 = (T_s\omega_\beta)^2-2\zeta_\beta T_s\omega_\beta+1$, $B_1=2\zeta_\beta T_s\omega_\beta-2$, $B_0 = 1$.

According to (12), when $\zeta_\beta \geqslant [4+(\omega_\beta T_s)^2]/(4\omega_\beta T_s)$, the poles of $G_{2\_PLF}(z)$ lie on or outside the unit circle. Define $\zeta_{\beta lim}= [4+(\omega_\beta T_s)^2]/(4\omega_\beta T_s)$. When $\zeta_\beta < \zeta_{\beta lim}$, the poles of $G_{2\_PLF}(z)$ lie inside the unit circle. To ensure that $G_{2\_PLF}(z)$ is designed to be stable, the value of ζ_β must satisfy $\zeta_\beta < \zeta_{\beta lim}$. When $\omega_\beta = \omega_s/2$, the corresponding $\zeta_{\beta lim}$=1.103.

After phase compensation by $G_{2\_PLF}(z)$, the phase of the equivalent impedance $\angle Z_{eq}$ is given by:

This article has been accepted for publication in a future proceedings of this conference, but has not been fully edited. Content may change prior to final publication.
Citation information: DOI: 10.1109/CPERE65146.2025.11240016, 2025 IEEE Conference on Power Electronics and Renewable Energy (CPERE)

$$\angle Z_{\mathrm{eq}}\left(e^{j\omega T_s}\right)=\arctan\frac{A_2\sin\omega T_s-A_0\sin\omega T_s}{A_2\cos\omega T_s+A_1+A_0\cos\omega T_s}-\arctan\frac{B_2\sin 2\omega T_s+B_1\sin\omega T_s}{B_2\cos 2\omega T_s+B_1\cos\omega T_s+B_0} \tag{13}$$

By substituting the parameters $\omega_\alpha = \omega_s/4$ and $\omega_\beta = \omega_s/2$, and $\zeta_{\beta\mathrm{lim}}$ = 1.103, and initially setting ζ_α=0.85. Fig. 7 shows the value range of ζ_β that ensures a positive equivalent resistance R_{eq}>0 after phase compensation by $G_{2\_\mathrm{PLF}}(z)$, based on (13).

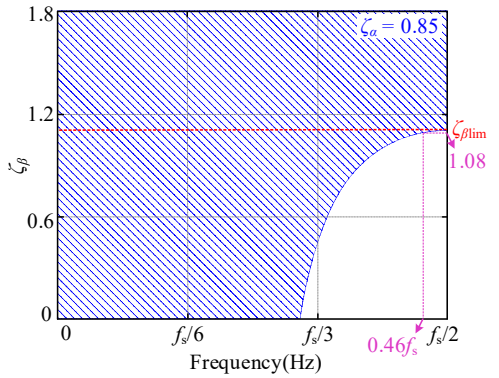

Fig. 7 Value range of ζ_β that satisfy R_{eq} >0

From Fig. 7, the shaded area represents the region where the equivalent resistance R_{eq}>0. When $\zeta_\beta > \zeta_{\beta\mathrm{lim}}$, the equivalent resistance R_{eq}>0 is valid within the frequency range (0, f_s/2), but $G_{2\_\mathrm{PLF}}(z)$ becomes unstable. To ensure that $G_{2\_\mathrm{PLF}}(z)$ is stable, ζ_β must be less than $\zeta_{\beta\mathrm{lim}}$. As ζ_β decreases, the frequency range that satisfies R_{eq}>0 becomes narrower. Therefore, ζ_β should be chosen as close as possible to $\zeta_{\beta\mathrm{lim}}$ while maintaining some margin. In this study, ζ_β = 1.08 is selected, and the frequency range where R_{eq}>0 is (0, 0.46f_s).

Fig. 8 shows the magnitude of the equivalent resistance R_{eq} after compensation by $G_{2\_\mathrm{PLF}}(z)$ for different values of ζ_α. It can be observed that the frequency range satisfying R_{eq}>0 is (0, 0.46f_s). As the damping ratio ζ_α increases, the magnitude of R_{eq} in the high-frequency range increases significantly, while the magnitude in the low-frequency range remains unaffected. Therefore, ζ_α=1 is selected.

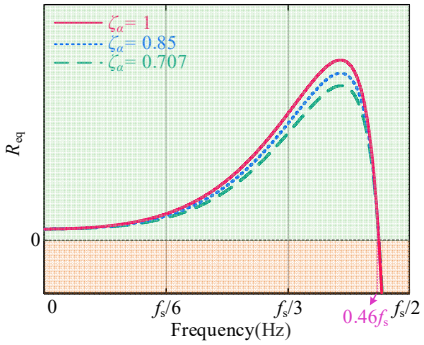

Fig. 8 Comparison of R_{eq} magnitude with different values of ζ_α.

B. *Stability Analysis of ICFB-AD By Phase Compensation*

Experimental parameters are listed in TABLE I. The grid impedance L_g is assumed to be 0μH or 6mH, respectively. L_1= 230μH is defined as 1.0 p.u. By selecting L_1=1.0 p.u. and L_g= 6mH, the minimum value of f_r, denoted as f_{r_min}, equals 0.23f_s. It is assumed that the inductance L_1 can decrease to 0.5p.u. By selecting L_1=0.5 p.u. and L_g= 0μH, the maximum value of f_r, denoted as f_{r_max}, equals 0.39f_s.

TABLE I. PARAMETERS OF THE EXPERIMENTAL PROTOTYPE

Parameter	Value
DC-side voltage V_{dc}	360 V
Grid phase voltage v_g	110 V(RMS) / 50 Hz
Inverter-side inductor L_1	230 μH
Grid-side inductor L_2	250 μH
Filter capacitor C_f	3.7 μF
Grid impedance L_g	6 mH
Rated Power P	6.6 kW
Switching frequency f_{sw}	24 kHz
Sampling frequency f_s	24 kHz

From Fig. 2(a), the open-loop transfer function of the ICFB-AD system with λ = 0.5 is given by:

$$T_{\mathrm{plant}}(z)=\frac{G_i(z)\cdot G_{iL1}(z)}{1+T_{\mathrm{AD\_open\_0.5}}(z)} \tag{14}$$

From (14), Fig. 9 shows the open-loop Bode plot of the ICFB-AD control system after phase compensation by $G_{2\_\mathrm{PLF}}(z)$.

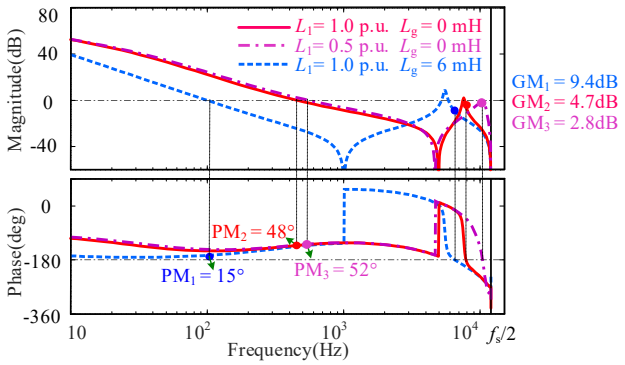

Fig. 9 Open loop bode diagram of the ICFB-AD with compensation by $G_{2\_\mathrm{PLF}}(z)$

As shown in Fig. 9, the ICFB-AD control system remains stable despite variations in LCL filter parameters. When the grid-side inductance L_g fluctuates to 6 mH, although the resonance peak exceeds the 0 dB line, the control system maintains sufficient stability margin due to the considerable low-frequency phase lead introduced by $G_{2\_\mathrm{PLF}}(z)$. Even when the inverter-side inductor L_1 varies to 0.5 p.u., the system remains stable. Under the proposed control strategy, the grid-connected inverter exhibits good stability and strong robustness against variations in both grid impedance and filter inductance parameters.

V. EXPERIMENTAL RESULTS

A 6.6 kW three-phase LCL GCI was built and tested in the laboratory, and parameters are listed in TABLE I. Fig. 10 shows experimental results and comparison, where i_{L2_A}, i_{L2_B}, i_{L2_C} and v_{PCC_AB} represent three-phase grid currents and grid line voltages, respectively.

Fig. 10 (a) shows experimental results with L_1= 1.0p.u. and L_g= 0μH. It can be seen that three-phase grid currents are stable by enabling the proposed ICFB-AD scheme, and a 7.6 kHz resonance of three-phase grid currents is generated by enabling the proportional ICFB-AD scheme. When the resonance frequency is 7.6 kHz, it falls within the negative-resistance frequency region of the equivalent resistance R_{eq}. As a result, the proportional ICFB-AD scheme provides negative damping.

This article has been accepted for publication in a future proceedings of this conference, but has not been fully edited. Content may change prior to final publication.
Citation information: DOI: 10.1109/CPERE65146.2025.11240016, 2025 IEEE Conference on Power Electronics and Renewable Energy (CPERE)

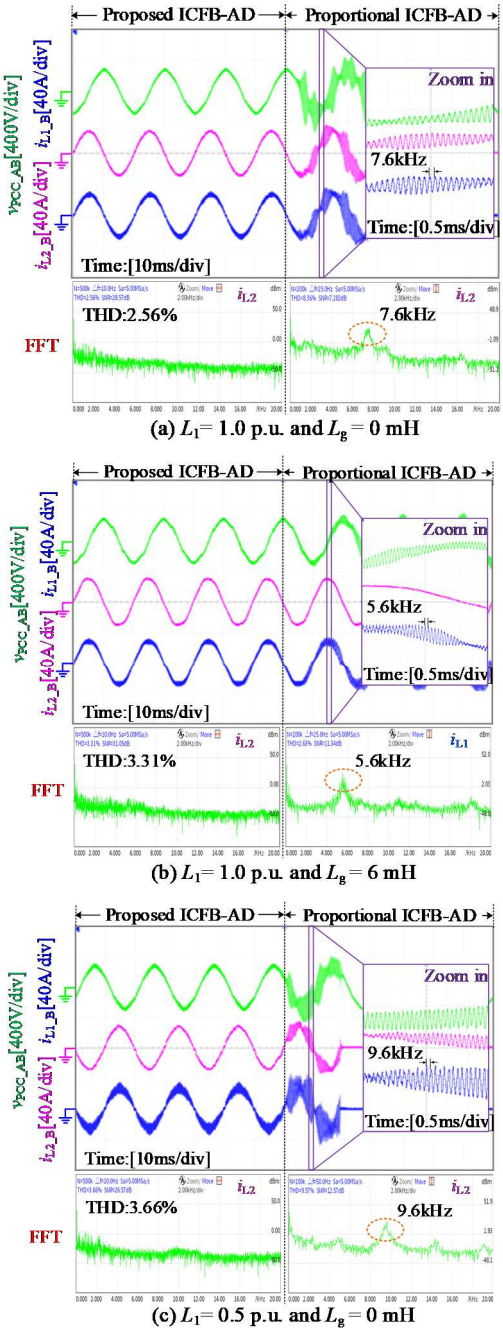

Fig. 10 Experimental results with the proposed ICFB-AD method and the proportional ICFB-AD method

Fig. 10 (b) shows the steady-state waveform of three-phase grid currents with L_1= 1.0p.u. and L_g= 6 mH. It can be seen that the grid-connected inverter remains stable under the proposed ICFB-AD scheme. However, after switching to proportional ICFB-AD, a 5.6 kHz resonance occurs in the grid current. It indicates that since f_r is close to $f_s/4$, the damping effect provided by the proportional ICFB-AD is insufficient.

Fig. 10 (c) shows the experimental result with L_1= 0.5p.u. and L_g= 0 mH. It can be seen that, the grid-connected inverter is stable by enabling the proposed scheme, while the proportional ICFB-AD scheme causes a 9.6kHz resonance of grid currents. Thus, since f_r= 9.6 kHz is higher than $f_s/3$, the proportional ICFB-AD still leads to the instability of the grid-connected inverter. It demonstrates that the proposed ICFB-AD scheme exhibits strong robustness against variations of inverter-side inductance and grid impedance.

VI. Conclusion

This paper proposed an improved ICFB-AD control scheme by placing a *s*-domain second-order unstable PLF in series with the feedforward link. Experimental results and theoretical analysis demonstrate that the proposed scheme has the following advantages.

1) The *z*-domain magnitude-frequency response of the ICFB-AD loop (λ = 0.5) is infinitesimal with f approaching the Nyquist frequency. It is shown that this characteristic can suppress the high-frequency gain of the digital filter, thereby simplifying the stability design of the damping inner loop.

2) The GCI is stable with f_r varied in a wide range of $(0,0.46f_s)$, which indicates that high robustness against the variation of the filter inductance and the grid impedance is guaranteed by the proposed ICFB-AD scheme.

Additionally, it is notable that the proposed ICFB-AD scheme offers a simple and cost-effective solution for the stable operation of LCL-filtered GCI, making it applicable to distributed renewable energy generation systems.

References

[1] T. Liu, J. Liu, Z. Liu and Z. Liu, "A Study of Virtual Resistor-Based Active Damping Alternatives for LCL Resonance in Grid-Connected Voltage Source Inverters," *IEEE Trans. Power Electron.*, vol. 35, no. 1, pp. 247-262, Jan. 2020.

[2] P. Pan, X. Ruan, C. Bao, W. Li and X. Wang, "Capacitor-Current-Feedback Active Damping With Reduced Computation Delay for Improving Robustness of LCL-Type Grid-Connected Inverter," *IEEE Trans. Power Electron.*, vol. 29, no. 7, pp. 3414-3427, July 2014.

[3] Hu M, Hua W, Xiao H, et al, "Fast Current Control Without Computational Delay by Minimizing Update Latency," *IEEE Trans. Power Electron.*, vol. 36, no. 11, pp. 12207-12212, Nov. 2021.

[4] X. Zhang, P. Chen, C. Yu, F. Li, H. T. Do and R. Cao, "Study of a Current Control Strategy Based on Multi-sampling for High-Power Grid-Connected Inverters With an LCL filter," *IEEE Trans. Power Electron.*, vol. 32, no. 7, pp. 5023-5034, July 2018.

[5] I. Z. Petric, P. Mattavelli and S. Buso, "Feedback Noise Propagation in Multisampled DC–DC Power Electronic Converters," *IEEE Trans. Power Electron.*, vol. 37, no. 1, pp. 150-161, Jan. 2022.

[6] S. He, D. Zhou, X. Wang and F. Blaabjerg, "Aliasing Suppression of Multisampled Current-Controlled LCL-Filtered Inverters," *IEEE J. Emerg. Sel. Topics Power Electron.*, vol. 10, no. 2, pp. 2411-2423, April 2022.

[7] S. He, D. Zhou, X. Wang, Z. Zhao and F. Blaabjerg, "A Review of Multisampling Techniques in Power Electronics Applications," *IEEE Trans. Power Electron.*, vol. 37, no. 9, pp. 10514-10533, Sept. 2022.

[8] D. Yang, X. Ruan and H. Wu, "A Real-Time Computation Method With Dual Sampling Mode to Improve the Current Control Performance of the LCL-Type Grid-Connected Inverter," *IEEE Trans. Ind. Electron.*, vol. 62, no. 7, pp. 4563-4572, July 2015.

[9] L. Lin, X. Ruan, H. Zhang and L. Wu, "A Generalized Real-Time Computation Method With Dual-Sampling Mode to Eliminate the Computation Delay in Digitally Controlled Inverters," *IEEE Trans. Power Electron.*, vol. 37, no. 5, pp. 5186-5195, May 2022.

[10] Y. Tu, J. Liu, Z. Liu, D. Xue and L. Cheng, "Impedance-Based Analysis of Digital Control Delay in Grid-Tied Voltage Source Inverters," *IEEE Trans. Power Electron.*, vol. 35, no. 11, pp. 11666-11681, Nov. 2020.

[11] J. Liu, M. Yang and T. Wang, "Impedance-Based Stability Analysis of Grid-Tied Photovoltaic System With Superconducting Magnetic Energy Storage System," *IEEE Transactions on Applied Superconductivity*, vol. 31, no. 8, pp. 1-4, Nov. 2021.

[12] Z. Xin, X. Wang, P . C. Loh, and F. Blaabjerg, "Grid-current-feedback control for LCL-filtered grid converters with enhanced stability," *IEEE Trans. Power Electron.*, vol. 32, no. 4, pp. 3216-3228, Apr. 2017.

[13] Z. Xin, X. Wang, P. C. Loh and F. Blaabjerg, "Realization of Digital Differentiator Using Generalized Integrator For Power Converters,"

IEEE Trans. Power Electron., vol. 30, no. 12, pp. 6520-6523, Dec. 2015.

[14] T. Fang, S. Shen, L. Zhang, Y. Jin and C. Huang, "Capacitor Current Feedback With Phase-Lead Compensator to Eliminate Resonant Frequency Forbidden Region for LCL-Type Grid-Connected Inverter in Weak Grid," *IEEE J. Emerg. Sel. Topics Power Electron.*, vol. 9, no. 5, pp. 5581-5596, Oct. 2021.

[15] Q. Qian *et al*., "Coordinated Self-Tuning Implementation of Repetitive Control and Active Damping for 400 Hz Inverter against Filter Inductance Fluctuation," *IEEE Trans. Power Electron.*, vol. 39, no. 12, pp. 15520-15535, Dec. 2024.

[16] S. Li and H. Lin, "A Capacitor-Current-Feedback Positive Active Damping Control Strategy for LCL-Type Grid-Connected Inverter to Achieve High Robustness," *IEEE Trans. Power Electron.*, vol. 37, no. 6, pp. 6462-6474, June 2022.

[17] W. Chen, Y. Zhang, Y. Tu, K. Shen and J. Liu, "Active Damping Control for LCL Filters With Inverter-Side Current Feedback Only," *IEEE Trans. Power Electron.*, vol. 37, no. 9, pp. 10065-10069, Sept. 2022.

[18] Y. Cai, Y. He, H. Zhou and J. Liu, "Active-Damping Disturbance-Rejection Control Strategy of LCL Grid-Connected Inverter Based on Inverter-Side-Current Feedback," *IEEE J. Emerg. Sel. Topics Power Electron.*, vol. 9, no. 6, pp. 7183-7198, Dec. 2021.

[19] A. A. Nazib, D. G. Holmes and B. P. McGrath, "Self-Synchronizing Stationary Frame Inverter-Current-Feedback Control for LCL Grid-Connected Inverters," *IEEE J. Emerg. Sel. Topics Power Electron.*, vol. 10, no. 2, pp. 1434-1446, April 2022.

[20] D. Pan, X. Ruan, X. Wang, H. Yu and Z. Xing, "Analysis and Design of Current Control Schemes for LCL-Type Grid-Connected Inverter Based on a General Mathematical Model," *IEEE Trans. Power Electron.*, vol. 32, no. 6, pp. 4395-4410, June 2017.

[21] A. A. Nazib, D. G. Holmes and B. P. McGrath, "Self-Synchronizing Stationary Frame Inverter-Current-Feedback Control for LCL Grid-Connected Inverters," *IEEE J. Emerg. Sel. Topics Power Electron.*, vol. 10, no. 2, pp. 1434-1446, April 2022.

[22] E. Jury, Theory and Application of the *z*-Transform Method. Malabar, FL, USA: Krieger, 1973.